ADVANCED MATERIALS TECHNOLOGIES
www.advmattechnol.de

Transwell-Integrated 2 µm Thick Transparent Polydimethylsiloxane Membranes with Controlled Pore Sizes and Distribution to Model the Blood-Brain Barrier

*Mariia Zakharova, Martijn P. Tibbe, Lena S. Koch, Hai Le-The, Anne M. Leferink, Albert van den Berg, Andries D. van der Meer, Kerensa Broersen, and Loes I. Segerink**

Traditional Transwell inserts with track-etched 10 µm thick polymer membranes have been intensively used for studying cellular barriers. However, their thickness hampers direct cell-cell interaction between the adjacent cells which has been shown to critically influence the barrier formation. Therefore, here the effect of reduced distance between the cells by using fivefold thinner (2 µm) optically transparent polydimethylsiloxane (PDMS) membranes is studied and compared with polycarbonate (PC) membranes. The authors validate their applicability as an alternative substrate for the study of the blood–brain barrier by performing a monoculture of brain endothelial cells (hCMEC/D3) and co-culture with astrocytes in Transwells. The PDMS membranes supported the cellular protrusions through the well-defined pores and allowed control over cellular transmigration by varying the pore size. Cellular localization of tight and adherens junction proteins ZO-1, Claudin-5, and VE-cadherin is similar to PC membranes while their expression levels are affected as a function of membrane material and co-culture with astrocytes. Additionally, a permeability assay indicated tighter barrier formation on the PDMS membrane. These results suggest the potential use of 2 µm PDMS membranes for in vitro modeling of biological barriers with improved co-culture models and enhanced visibility of the cell culture.

1. Introduction

The study of biological barriers involves the use of one or more co-cultured cell types under conditions that provide a means to self-organize into a well-defined barrier with functionality that closely resembles that of in vivo biology. Porous membranes are widely used as a cell culture substrate in multicompartment in vitro models such as Transwell and Organ-on-chip (OOC).[1,2] Such models can provide an insight into biological signaling pathways, cell–cell interactions, and enable drug screening for diverse pathologies with the possibility to predict individual patient responses to drugs.

In most cases, the barrier function is mimicked using commercially available polycarbonate (PC), or polyethylene terephthalate (PET) 0.4–8 µm pore-sized membranes coated with extracellular matrix (ECM) proteins on which different cell types are cultured in two compartments.[3–9] For example, when modeling in vitro blood–brain barrier (BBB), the endothelial cells are co-cultured with astrocytes or glial cells attached to another side of the membrane.[10–13] It was found that direct contact between these adjacent cells plays a key role in barrier function with an increased tight junction, gene expression, and barrier tightness.[10,14–16] However, the PC or PET membranes form a physiologically irrelevant thick barrier (≈10 µm) inhibiting physical cell–cell interaction across the membrane and limit their potential to closely resemble the in vivo basement membrane which is suggested to be in the sub-micrometer range with a spatial and temporal variation.[17–19]Additionally, the random distribution of the pores created by track etching leads to undefined and underestimated pore sizes due to the interconnection of pores and limits the possibility of live-cell imaging using bright-field or phase-contrast microscopy.

This has led to the development of new generation membranes that allow closer resemblance of several in vivo membrane features. For example, the membranes from materials such as poly(ε-caprolactone) and poly(lactide-co-caprolactone) were successfully fabricated using electrospinning or solution casting with the thickness of 4 µm and 960 nm, respectively.[20,21] Despite the closer resemblance of the basement membrane physiology there is no control over pore distribution or size using these technologies. By using microelectromechanical systems (MEMS) fabrication technologies, it was possible to fabricate ultrathin membranes with thickness in the nanometer

M. Zakharova, M. P. Tibbe, L. S. Koch, H. Le-The, A. M. Leferink, A. van den Berg, A. D. van der Meer, K. Broersen, L. I. Segerink
University of Twente
Enschede 217 7500 AE, the Netherlands
E-mail: l.i.segerink@utwente.nl

The ORCID identification number(s) for the author(s) of this article can be found under https://doi.org/10.1002/admt.202100138.

DOI: 10.1002/admt.202100138

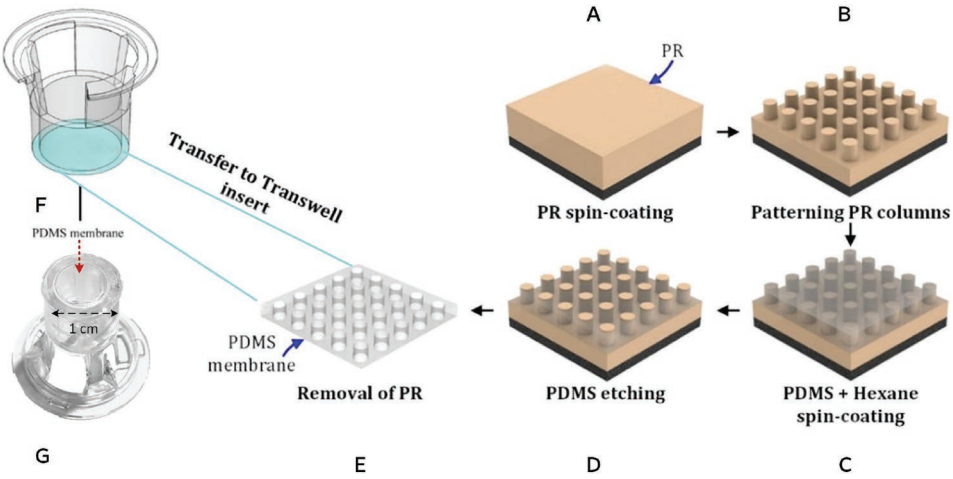

Figure 1. Schematic image of the fabrication process of the patterned porous PDMS membrane. A) A layer of positive photoresist (PR) is spin-coated onto an HMDS coated 4″ silicon wafer. B) The PR layer is patterned using photolithography resulting in a PR column array. C) A mixture of PDMS and hexane (2:5 weight ratio) is spin-coated over the PR column array. D) The residual PDMS layer is etched using reactive ion etching. E,F) The PDMS membrane is released by dissolving the PR layer and G) attached to the rim of a Transwell insert to fully replace the original PC membrane that was removed.

range and different pore sizes.[22–26] As the pore distribution and pore size are well controlled by the photolithography process, the cells experience a regular cell culture surface. Additionally, thinner membranes facilitate mechanotransduction between cells situated on adjacent sides of the substrate.[23,27] However, such inorganic membranes become extremely brittle with reducing thickness, and therefore the free-standing substrate area is limited and requires extra support.[28–30]

While membrane thickness critically determines factors such as cell–cell interaction, stiffness of the substrate was shown to affect cell proliferation, motility, and surface marker expression.[21,31–33] Cells sense the substrate on which they grow through focal adhesion points and generate signals based on the forces required to deform the matrix which is dependent on the elastic modulus of the substrate.[34,35] For comparison, silicon-based membranes have the elastic modulus in the hundred gigapascals range while the elastic modulus of the soft tissues (e.g., brain, heart, lung) is varying between 0.5–1 KPa.[36,37] Although this parameter is decreased for thinner substrates (e.g., Young's modulus of 2 nm-thick silicon nanomembrane is 3 GPa), it still significantly exceeds that found in vivo.[38] At the same time, PDMS membranes have a lower elastic modulus (≈1.3 MPa), compared to traditionally used PC (≈2–2.4 GPa) and PE (≈2–3 GPa) membranes thus resembling the biological membranes of soft tissues more closely.[39]

Recently, we reported the fabrication of porous 2 μm PDMS membranes with tunable thickness and pore size that can be used in cell culture and OOC research.[41,42] These membranes are optically transparent, enabling live-cell imaging by bright field and phase-contrast microscopy without the need for fluorescent markers. In this work, we focus on the characterization of our PDMS membranes by recreating a BBB using adapted Transwell inserts and studying how the reduced thickness influences the cell culture. For this, a co-culture of human cerebral microvascular endothelial cells (hCMEC/D3) and human astrocytes was used. The cell viability, immunofluorescent staining, protein expression, and permeability were compared to traditionally used Transwells with PC membrane. Improvement of Transwell systems to model the BBB would be instrumental to further their application in disease modeling and therapeutic studies.

2. Results and Discussion

2.1. Fabrication of a 2 μm Thick, 3 μm and 5 μm Pore-Sized PDMS Membrane

The BBB is comprised of a monolayer of tightly connected endothelial cells that line the blood microvessels in the brain.[43] This endothelial monolayer connects with other cell types including astrocytes and pericytes to collectively regulate BBB maintenance although their individual contributions remain under debate.[44–46] In vitro, BBB models are created on different pore seized membranes, ranging from nano- to few micron pore sizes.[47,48] Micropore organization and dimensions were shown to critically regulate processes such as cellular transmigration, permeability, and intercellular interaction.[10,49]

In this work, we used 3 and 5 μm spatially organized pore sizes with 30 μm pitch to facilitate contact between the two cell types cultured on different sides of the membrane. The porosity of the fabricated membranes is 2% in comparison to 8% in PC Transwell membranes. The pore sizes and porosities can be tuned by using the reported fabrication method (**Figure 1**), however, it is important to take into account the aspect ratio of 3:1 for the used positive photoresist.[41,42]

The success rate of transferring fabricated membranes to Transwells was more than 90%. After transfer, the membranes were evaluated for the absence of leakage from the edges of the Transwell, and, when needed, an additional layer of glue was applied to ensure a tight bond with the polystyrene rim of the Transwell insert. The complete fabrication of the membranes can be done in 1.5 days and around 60 Transwell membranes can be retrieved from one processed wafer.

Variation of the PDMS:hexane ratio, as well as the speed of spin-coating and the etching time, determine the final membrane thickness.[41] The thickness of the PDMS should be chosen such that the residual layer of PDMS on top of the pillars is relatively thin (nanometer range), resulting in a minimal time of dry etching. Analysis of the PDMS surface after etching using SEM-EDS showed some traces of sulfur (≈1.5 wt%), which should be kept minimal by reducing the etching time.

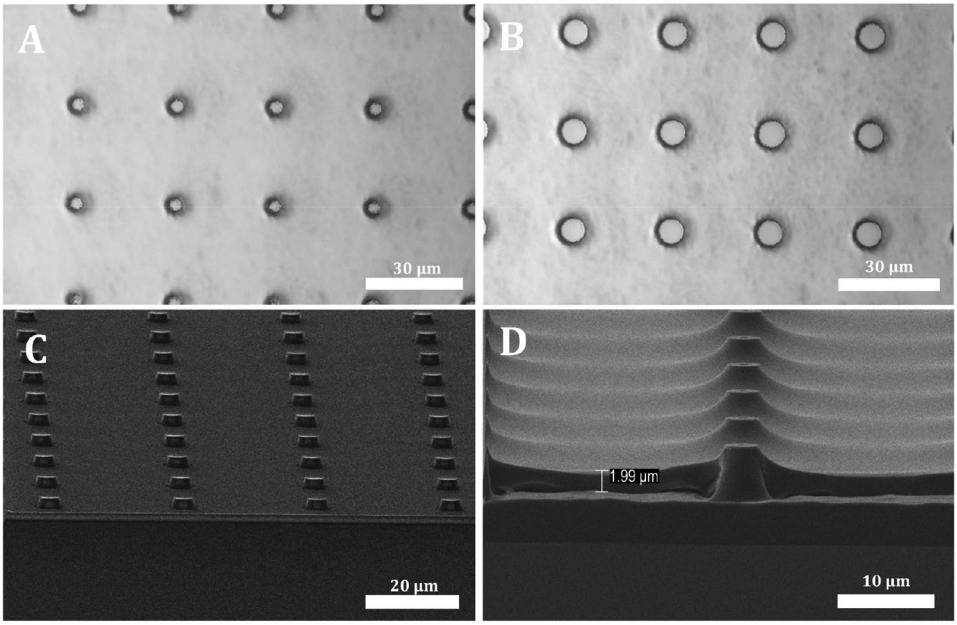

Figure 2. Bright-field and HR-SEM images of the PDMS membrane. A) A PDMS membrane with 3 µm pore diameter, and B) 5 µm pore diameter. C) An array of 5 µm PR pillars on a wafer. D) The membrane itself has a thickness of 2 µm after etching.

In this research, membranes with a thickness of ≈2 µm were fabricated (**Figure 2**). When a mask with 3 (Figure 2A) and 5 µm (Figure 2B) pore sizes is used, the actual pillar diameter turns out to be 2.69 ± 0.11 µm and 4.91 ± 0.17 µm, respectively. The final size of the pores is dependent on the thickness of the membrane as the used pillars are slightly tapered (Figure 2D). In this case, a thinner membrane results in larger pores.

2.2. The Culture of Cells on PDMS Membranes Allows Visualization by Phase-Contrast Imaging

Non-invasive monitoring of the cell culture is important to be able to continuously follow the cells' proliferation and monolayer formation. Unlike PC membranes, the fabricated PDMS membranes allow phase-contrast visualization of cultured cells without additional labeling (**Figure 3**). Due to the thickness of PC membranes and random distribution of the pores, the light is significantly scattered, thus, the state of the cells is often unknown before the end of the experiment when fluorescent staining is performed.[39] The light scattering is reduced in PDMS membranes due to well-defined pores with controlled pore spacing, therefore, allowing live mono- and co-culture (Figure 3C,D) imaging during the experimental time.

2.3. The Etching Process of PDMS Does not Affect Cell Viability upon Culturing on PDMS Membranes

To validate whether etching PDMS using sulfur hexafluoride (SF_6) and oxygen results in traces that are toxic to cells cultured on these membranes, the viability of hCMEC/D3 cells was evaluated using a live/dead assay (**Figure 4**). Endothelial cells formed a visual monolayer on both membranes over 5 days culture period.

Results from the live/dead viability assay showed that ≈98% of cells remained viable on both the PDMS and PC membranes independently from the pore size used. These results indicate that the etching process of the PDMS membrane was not harmful to the cells which were able to maintain high viability, similar to the cells cultured on the PC membrane.

The scattering of light due to randomly distributed pores on the PC membrane caused a varying degree of blurring which is seen in Figure 4B.

2.4. Endothelial Cells Protrude through the Membrane Pores

Generally, porous biological membranes, such as the BBB basement membrane, allow either direct contact between cells residing on the two sides of the substrate or signal transduction.[50,51] The proximity of the cell–cell interaction across the basement membrane is greatly facilitated by pore size and limited thickness of the membrane. While previous studies using conditioned medium (CM) from astrocytes showed that soluble factors play an important modulating role in endothelial response in co-culture, direct physical interaction was considered to be instrumental in inducing polarity of apical and basal compartments.[52–54]

Cell–cell contact of hCMEC/D3 cells and astrocytes and the ability of the cells to migrate through the different pore sizes were compared on PDMS and PC membranes (**Figure 5** for 5 µm pores and Figure S1, Supporting Information, for 3 µm pores). For this, the cell culture was performed for 5 days. A shorter culture period is insufficient to form a tight barrier while prolonged culture, exceeding 6 days, in static Transwell models may lead to overgrowth as reported previously.[55–57]

Apart from forming cellular protrusions (Figure 5B), cells were able to fully migrate through 5 µm pores and accumulate

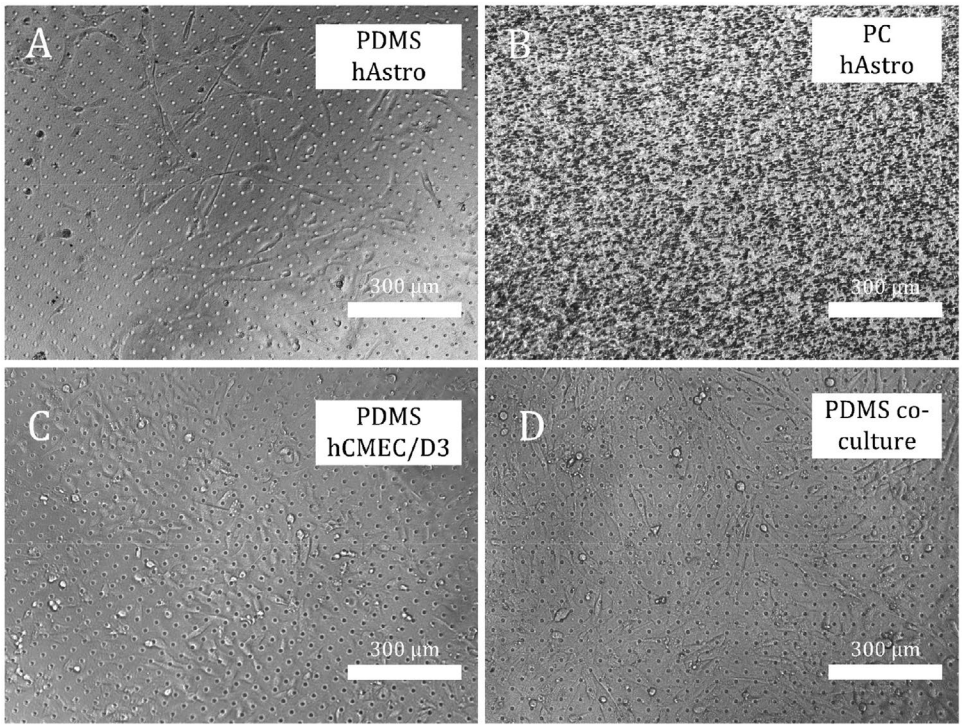

Figure 3. Phase-contrast images of astrocytes and hCMEC/D3 cells cultured on 5 µm pore-sized membranes. A) Astrocytes cultured for 10 h on a PDMS membrane, while B) on a PC membrane the astrocytes are not distinguishable because of a lack of membrane's transparency. C) hCMEC/D3 cells cultured overnight on PDMS membrane, and D) a co-culture of hCMEC/D3 cells and astrocytes on day 2 after hCMEC/D3 seeding. Cell morphological features can be distinguished on PDMS membranes: astrocytes are elongated compared to hCMEC/D3 cells which have cobble-stone-like morphology.

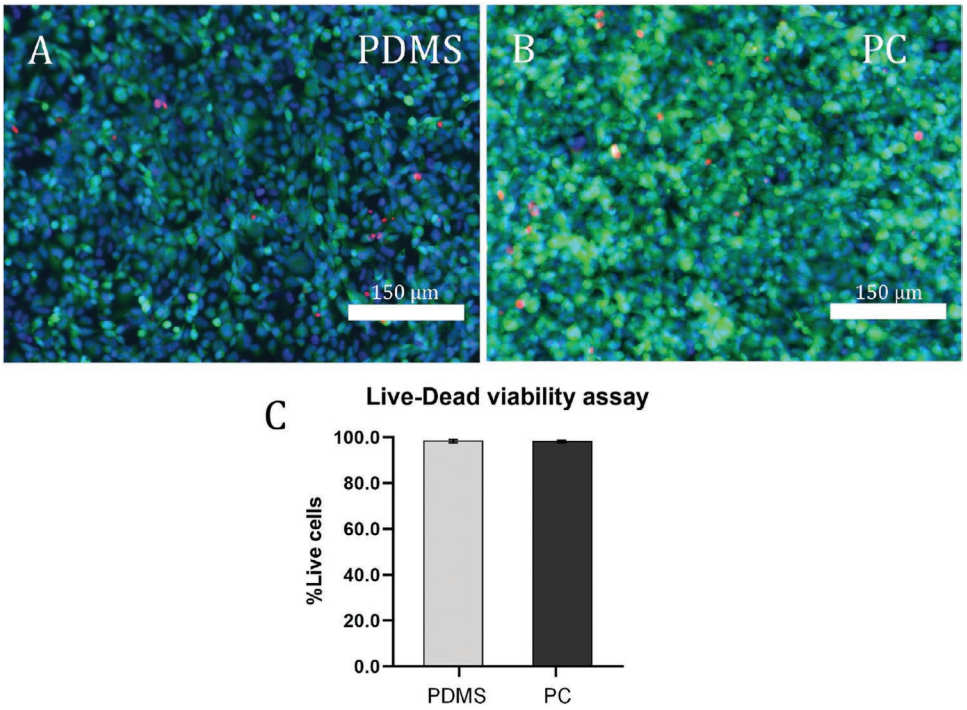

Figure 4. Live/dead viability assay after 5 days of hCMEC/D3 culture. A) PDMS membranes compared to B) PC membranes. Viable cells are stained with Calcein AM (green), whereas necrotic cells are stained using ethidium homodimer (red), and cell nuclei are stained with NucBlue. C) For both membrane types, the viability of endothelial cells was high (for PDMS 98.4 ± 0.6% and for PC 98.7 ± 0.2%, $n = 3$). The number of live and dead cells is counted using the "find maxima" method in ImageJ.

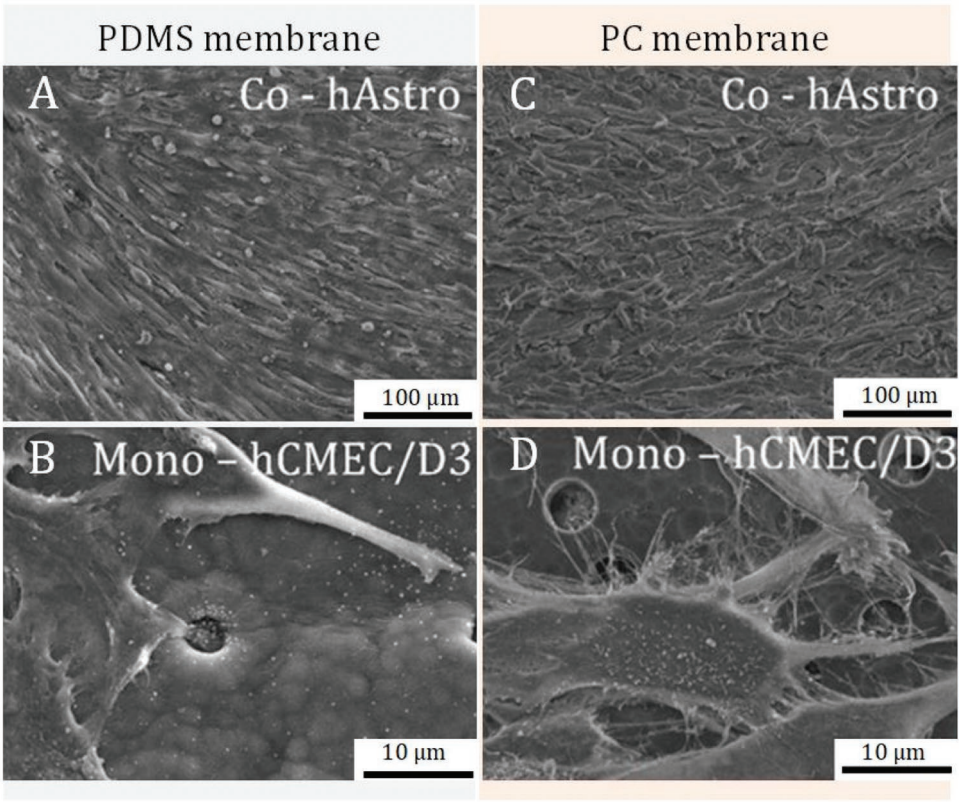

Figure 5. SEM images of hCMEC/D3 cells and human astrocytes cultured on 5 µm pore-sized PDMS and PC membranes. A) A layer of astrocytes characterized by elongated morphology. B) A zoom-in of the endothelial cell layer shows that protrusions of the cells extending into the pores. C) Astrocytes grown on the on PC membrane, however, the cells had different morphology compared to those grown on PDMS suggesting endothelial transmigration from another side of the membrane. D) A zoom-in on hCMEC/D3 cells covering the pores.

on the other side of PDMS membrane (Figure S2, Supporting Information). This is in accordance with other studies, where hCMEC/D3 cells were shown to be able to migrate through pores exceeding 3 µm in dimension.[11] Although cellular migration is of interest to study cancer cell extravasation or brain leukocyte infiltration, it is important to avoid the second non-physiological endothelial layer formation, therefore, we focused on 3 µm pore size membranes.

It was found that despite using a smaller pore size, hCMEC/D3 cells were able to migrate through the 3 µm pores on PC membranes while the use of PDMS membranes inhibited cellular transmigration (Figure S3, Supporting Information). The random pore distribution, and thus potential overlap of pores in PC membranes leads to a bigger size of the pores thus allowing transmigration of cells.

2.5. Astrocytes and hCMEC/D3 Cells Co-Cultured on a PDMS and PC Membranes

HCMEC/D3 and human astrocytes were co-cultured on PDMS or PC membranes to study the interaction between these two cell types. It is suggested that for the development of a functional barrier, interplay of the endothelial layer with astrocytes may be of key importance.[43,52,53] Cellular interplay across the basement membrane can consist of direct contact between the cell types or be facilitated by a reduced distance between the cell types allowing for more efficient paracrine signaling as the strength of the paracrine signal is related to distance.[58]

To study the influence of the reduced distance between astrocytes and endothelial cells in co-culture Transwell conditions, the expression of tight junction proteins (ZO-1, Claudin-5) and an adherens junction protein (VE-Cadherin) were assessed on the 5th day of culture on 3 µm pore-sized PDMS and PC membranes using immunostaining (**Figure 6** and Figure S4, Supporting Information). Upon culturing on PC and PDMS membranes, hCMEC/D3 cells showed similar primarily cytoplasmic ZO-1 (TJP1) cellular distribution on both PDMS and PC membranes.

These observations contradict previous studies of ZO-1 to primarily reside at the peripheral membrane as a result of its function in tight junction assembly.[59,60] However, ZO-1, apart from an interaction site for transmembrane proteins, also contains a C-terminal actin-binding site and forms phase-separated cytosolic clusters.[61–63] Moreover, ZO-1 localization in endothelial cells depends on several factors and one of them is the stiffness of the substrate, suggesting that extracellular matrix impacts the mechanotransduction of tight-junction structures.[57,64–66] To test whether the stiffer substrate will lead to localized tight junctions, we also seeded hCMEC/D3 on a glass chamber slide (Thermo Scientific Nunc Lab-Tek II Chamber Slide). The immunofluorescent staining of ZO-1 after 5 days of culture showed

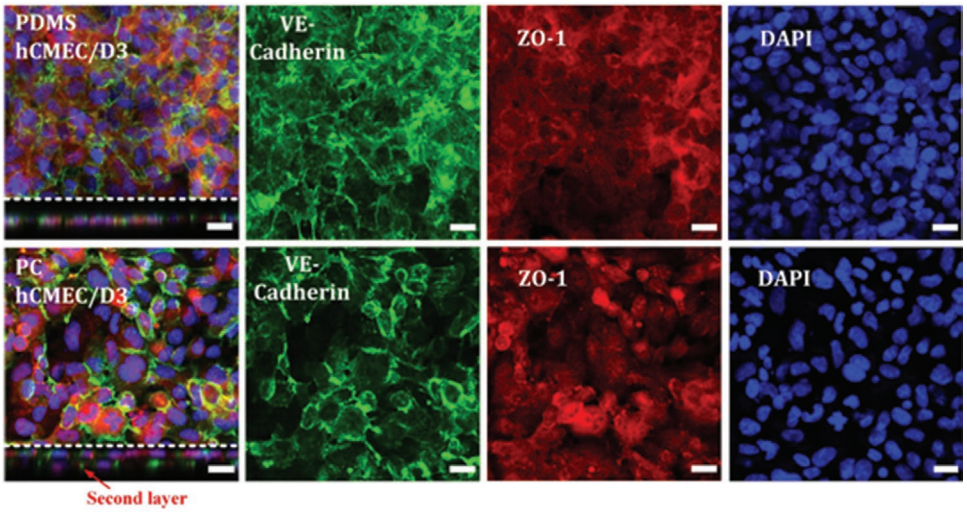

Figure 6. Comparison of immunostaining of adherens junction VE-Cadherin (Alexa Fluor 488, green), tight junction protein ZO-1 (Alexa Fluor 647, red), and cell nuclei (NucBlue, blue) on PDMS and PC membranes after 5 days of monoculture. HCMEC/D3 cells seeded in the upper compartment show a cobblestone morphology and express ZO-1 and VE-Cadherin on both membranes, although the localization of ZO-1 is slightly more specific on PC membranes. Besides, a second layer of the cells was observed on the other side of the 3 µm PC membrane, while on PDMS a continuous cellular monolayer was seen only on one side of the membrane. Scale bars represent 20 µm.

more peripheral localization of protein compared to PDMS and PC membranes (Figure S5, Supporting Information).

Interestingly, co-culture of hCMEC/D3 cells with astrocytes substantially modified cellular localization of ZO-1 to primarily plasma membrane-associated when cultured both on PC and PDMS membranes (**Figure 7**). Such changes in ZO-1 localization have been reported as a function of astrocyte co-culture or astrocyte-derived CM.[6,12,67,68]

In co-culture models, astrocytes were first seeded on the opposite side of the membrane. As astrocytes sediment on the surface of the membrane, it was expected that hCMEC/D3 seeded at a later stage will not be able to migrate to the astrocytic compartment. However in Figure 7, for cells grown on a PC membrane, ZO-1 staining was also visible in the astrocyte compartment, evidencing that hCMEC/D3 cells were able to protrude through the pores.

2.6. Endothelial Tight Junction Protein Expression Levels are Differentially Affected by Membrane Type and Co-Culture with Astrocytes

Numerous studies showed that astrocytes critically regulate BBB function.[54,69,70] In vitro, co-culture with astrocytes and

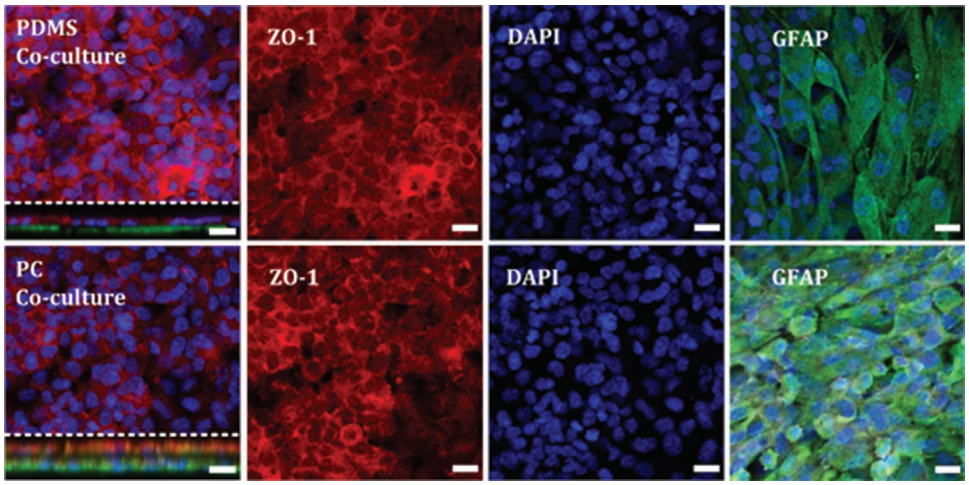

Figure 7. Immunofluorescent staining of ZO-1 (Alexa Fluor 647, red) and GFAP (Alexa Fluor 488, green) of an hCMEC/D3 and astrocyte co-culture on PDMS and PC membranes. Astrocytes cultured on both types of membranes are GFAP-positive but characteristic astrocyte elongated morphology were primarily observed when cultured on PDMS membranes. While the astrocytic compartment of cells grown on PDMS membranes is ZO-1 negative, the astrocytic compartment of PC membranes shows some degree of ZO-1 positive staining suggesting transendothelial migration through PC membranes. Cell nuclei (NucBlue, blue). Scale bars represent 20 µm.

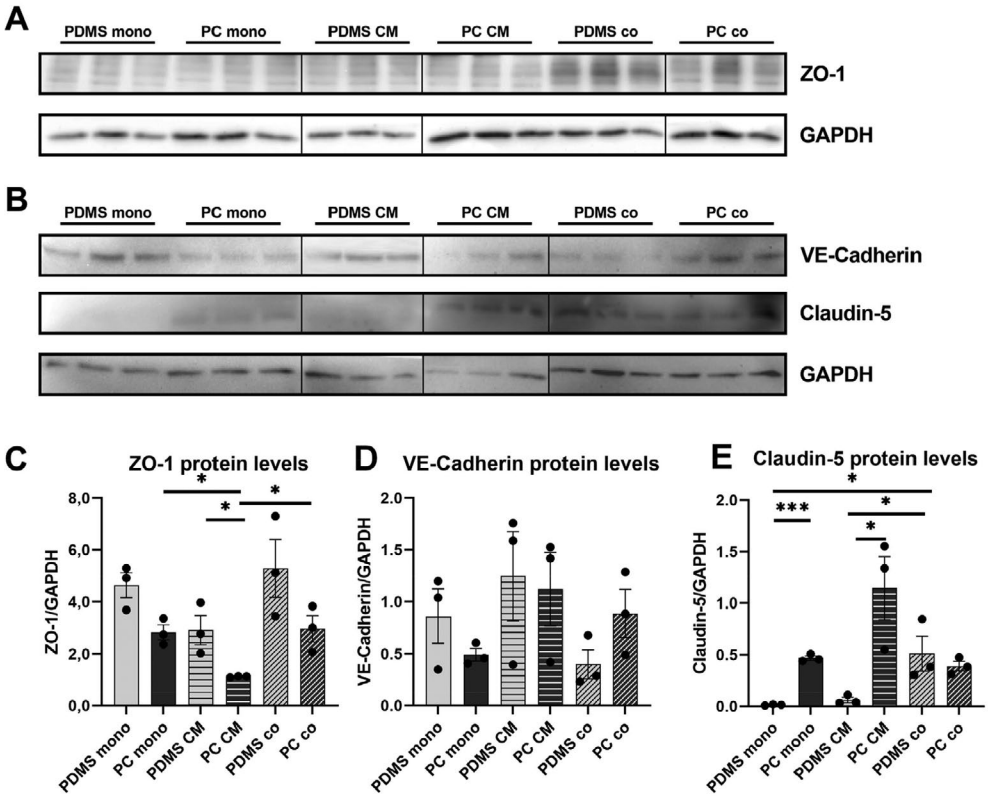

Figure 8. Immunoblot analysis presenting expression levels of relevant tight and adherens junction proteins in hCMEC/D3 grown under 3 different culture conditions (monoculture, culture with astrocyte-conditioned medium (CM), and co-culture with astrocytes). A) Immunoblot of ZO-1 expression. B) Immunoblot of expression of VE-Cadherin and Claudin-5. Dividers in (A) and (B) indicate where blot was stitched. C–E) Relative quantification of normalized expression levels of ZO-1 (C), VE-Cadherin (D), and Claudin-5 (E). Data are expressed as means ± SEM. $n = 3$. $^{*}p < 0.05$ and $^{***}p < 0.001$ (ANOVA).

substrate characteristics were previously shown to affect endothelial expression levels of tight junction proteins.[16,64,71] Based on these observations we measured endothelial expression levels of ZO-1, Claudin-5, and VE-cadherin cultured on PC and PDMS membranes in co-culture with astrocytes (**Figure 8**).

Results showed that ZO-1 expression levels were lower for hCMEC/D3 cells cultured on PC membranes compared to PDMS membranes. On the contrary, Claudin-5 expression was significantly lower for monocultures on PDMS compared to PC membranes ($n = 3$, $p = 2.8 \times 10^{-5}$) and in cultures with the addition of CM ($n = 3$; $p = 0.024$). The VE-cadherin expression levels did not significantly differ for hCMEC/D3 cells cultured on both membranes although it was previously shown that VE-Cadherin depends on the substrate stiffness, leading to increased cell contractility and gap formation.[72] These differential expression patterns of the three tight junction proteins tested are possibly the result of the known different transcriptional pathway regulation of these three tight junction proteins.[73]

Regulation of tight junction protein expression levels by endothelial cells may require direct physical interaction with astrocytes in the BBB. To address this question, we compared tight and adherens junction protein expression levels by hCMEC/D3 cells in the absence of astrocytes but upon exposure with astrocytic CM as well as in the presence of co-cultured astrocytes. Astrocytic soluble factors and soluble heat-labile protein aqueous factors have been suggested in the past to regulate endothelial tight junction formation and barrier integrity.[74] Examples of such reported factors are sonic hedgehog, WNT/β-catenin, transforming growth factor β, bone morphogenetic proteins, angiopoietins, or semaphorins that all affect BBB integrity.[75] However, there was no significant effect of CM detected for ZO-1, VE-Cadherin, and Claudin-5 expression for PDMS monoculture while on PC membranes, ZO-1 expression was downregulated upon CM ($n = 3$, $p = 0.028$). Similar results were shown previously, where the addition of CM did not enhance barrier properties of endothelial cells.[76]

Although cellular localization was affected by the presence of astrocytes (Figure 7), western blot analysis showed that co-culture with astrocytes non-significantly induced hCMEC/D3 expression of ZO-1 and downregulated VE-cadherin on both PDMS and PC membranes. The significant effect of co-culture compared to monoculture was seen for Claudin-5 expression on PDMS membranes ($n = 3$, for mono: $p = 0.027$ and CM: $p = 0.041$) while no such trend was detected for PC cultures. The observed non-significant increase in Claudin-5 expression levels on PC membranes are consistent with previous studies, where it was shown that the addition of astrocytes in contact/non-contact way does not lead to an increased Claudin-5 expression in b.End3 cells.[77] Overall,

these results may suggest that direct interaction between endothelial cells and astrocytes critically regulates tight junction formation.

2.7. Biological Barrier Permeability

Cell layer integrity can be measured by establishing the permeability of certain substances. We performed permeability experiments on day 5 of hCMEC/D3 culture on 3 µm pore size (PDMS and PC) membranes in mono- and co-culture conditions. Here we used fluorescently labeled dextran (20 kDa) which was added to the top compartment of the Transwell inserts and the fluorescent intensity in the bottom compartment was measured over time. Because the used PC and PDMS membranes have different porosities, the measurements were normalized to the permeability of empty substrates.

The permeability results for 20 kDa indicated that the hCMEC/D3 cell layer grown on PC membranes was more permeable compared to the barrier formed on the PDMS membrane. Despite the endothelial cell migration to another side of the PC membrane and formation of the second layer observed with immunostaining (Figures 6 and 7), the permeability rate was higher for both mono and co-cultures on PC membrane (**Figure 9**, for PC P_e mono- $3.08 \cdot 10^{-7} \pm 4.61 \cdot 10^{-8}$ cm s^{-1}, P_e co-culture $2.27 \cdot 10^{-7} \pm 4.86 \cdot 10^{-8}$ cm s^{-1} while for PDMS, P_e for mono $1.67 \cdot 10^{-7} \pm 4.10 \cdot 10^{-8}$ cm s^{-1}, and for co-culture $3.83 \cdot 10^{-7} \pm 2.07 \cdot 10^{-8}$ cm s^{-1}). The effect of co-culture with astrocytes was significant for hCMEC/D3 cells seeded on PDMS membrane demonstrating a decreased permeability rate and is not significant but still detectable for cells seeded on PC membrane. The permeability values presented here are lower than that normally observed for hCMEC/D3 culture however there are in line with other BBB models.[78,79]

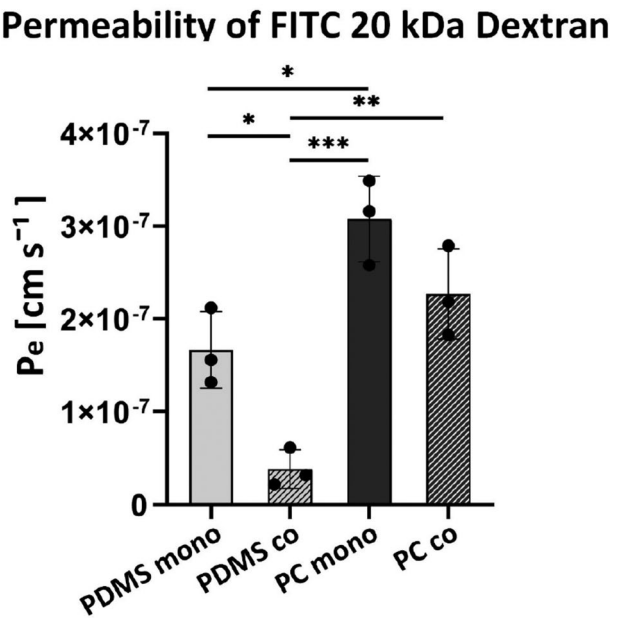

Figure 9. The endothelial permeability results indicated tighter barrier formation on PDMS membrane (blue bar) compared to PC (red bar). The astrocytes affected the permeability on both membranes, however, the change was significant for PDMS membranes. The bars represent mean with ±SD, $n = 3$, $*p < 0.05$, $**p < 0.01$, and $***p < 0.001$ (ANOVA).

3. Conclusion

We presented 2 µm thick optically transparent PDMS membranes that can be incorporated into Transwell systems for blood brain barrier modeling with improved cell–cell contact. The fabrication method of these membranes allows for precise control of pore size and membrane thickness which is not possible using a track-etched PC membrane. HCMEC/D3 cells cultured on the PDMS membrane showed comparable viability levels and protein (ZO-1, vascular endothelial cadherin [VE-Cadherin], and Claudin-5) expression compared to cultures on the PC membrane. The uniformity and controlled size of the pores allowed regulation of the cellular transmigration which was not possible using PC membranes. Moreover, the PDMS membrane enabled the formation of cellular protrusions suggesting possible cellular contact between hCMEC/D3 and astrocytes. Interestingly, the effect of adding astrocytes to the hCMEC/D3 culture was detectable for both membranes, but only permeability studies on the PDMS membrane showed a significant difference between mono and co-culture models. Finally, we detected elevated ZO-1 expression of hCMEC/D3 cells cultured on PDMS membrane, while Claudin-5 expression was downregulated. These results suggest that reduced membrane thickness is beneficial for cell–cell communication and the formation of a tight barrier even though the substrate's mechanical properties may also influence the cell behavior. Therefore additional functional studies have to be performed in the future. Ultimately, these PDMS membranes are meant to be used as substrates in OOC systems for modelling different barriers. They can be incorporated inside PDMS-based chips using only plasma activation without additional glues and without potentially harmful chemical surface modifications. Additionally, the PDMS membranes can be stretched for mechanical actuation of the barrier models such as lung and gut on a chip. Therefore, these membranes have great potential in facilitating improved biological barrier models and their studies.

4. Experimental Section

Membrane Fabrication: The PDMS membranes were fabricated as previously described.[42] Briefly, a thin hexamethyldisilazane (HMDS) was spin-coated onto a silicon wafer (Si) (525 µm thick, Okmetic, Finland) to increase the adhesion of the photoresist (PR) with the wafer surface. A 10 µm thin layer of positive PR (AZ 10XT, MicroChemicals, Germany) was spin-coated onto the HMDS coated Si wafer at 2000 rpm for 60 s. The Si wafer was baked at 110 °C for 3 min on a hotplate. The PR was exposed for 17 s with an intensity of 12 mW cm^{-2} using a mask alignment system (EVG620, EV Group, Austria), with a quartz photomask containing chromium circles of 3 and 5 µm in diameter. The Si wafer was then developed in an OPD4246 developer for 6 min and rinsed with de-ionized (DI) water, leaving free-standing PR column arrays on the wafer (Figure 1).

A degassed solution of PDMS prepolymer with curing agent (weight ratio 10:1) (Sylgard 184 Silicone elastomer kit, Dow Corning, MI, USA) was mixed with hexane at a 2:5 (PDMS:hexane) weight ratio to make the solution suitable for spin coating. The PDMS and hexane solution was spin-coated over the PR column array at 4000 rpm for 1 min. After

spinning, the PDMS membrane was cured at 60 °C for at least 12 h to remove all the hexane. Due to the spin-coating process, a thin residual layer of PDMS remains on the top of the columns thus resulting in a non-porous PDMS membrane.[41] To open the pores, a plasma etching process using a parallel plate reactive ion etching system (in-house built TEtske system, Nanolab University of Twente, the Netherlands) at 47 sccm SF_6, 17 sccm O_2, 50 mTorr, and 100 W was performed. Scanning electron microscopy energy-dispersive X-ray spectrometry (SEM-EDX) was used to obtain elemental quantitative data of the PDMS membrane surface after the plasma etching process.

It is worth mentioning that the membrane thickness down to 900 nm can be tuned by changing the etching time, however, such a thin membrane is difficult to handle. The membrane thickness was determined from images captured by using a high-resolution scanning electron microscope (HR-SEM, FEI Sirion microscope). SEM images were taken at a 5 kV acceleration voltage and a spot size of 3.

To use the fabricated PDMS membrane for cell culture, the original membrane of the Transwell insert (6.5 mm Transwell, with 3.0 (2×10^6 pores cm^{-2}) and 5.0 μm (4×10^5 pores cm^{-2}) pore sizes, Corning, NY, USA) was removed and replaced with this PDMS membrane. For this, uncured PDMS (pre-polymer: curing agent, 10:1 weight ratio) was used as a glue between the rim of the insert and the Si wafer with the membrane. After attaching the Transwell insert to the membrane, the PDMS glue was cured at 60 °C for 3 h. The membrane was released from the silicon substrate by dissolving both the PR columns as well as the PR sacrificial layer underneath the columns in a mixture of acetone and ethanol (100%) at a 70:30 v/v ratio. The released PDMS membranes were sterilized by immersing in ethanol (70% v/v) for 1 h. This step also reduces the amount of potentially toxic traces of other organic solvents to harmless levels. Prior to cell culture, the membranes were washed (3×) with 1× phosphate-buffered saline (PBS, Merck, Germany) to remove traces of ethanol.

Cell Culture and Analysis: In this work, both monocultures of only endothelial hCMEC/D3 cells (passage 30–35, Merck Millipore, the Netherlands) and co-cultures of hCMEC/D3 cells and astrocytes (passage 2–5, 3H Biomedical AB, Uppsala, Sweden) were used. Membranes were prepared for cell seeding by coating them for 1 h at 37 °C with 100 μg mL^{-1} collagen type I (rat tail, Corning Inc., USA) in PBS. For the monoculture, hCMEC/D3 cells were seeded on top of the Transwell-mounted PDMS membranes and commercially available Transwell systems with PC membranes. For this, hCMEC/D3 cells were resuspended at a 15×10^4 cells mL^{-1} concentration in endothelial cell growth medium (EGM, Sigma-Aldrich Chemie GmbH, Steinheim, Germany). A volume of 100 μL hCMEC/D3 cell suspension was pipetted on top of the collagen-coated PDMS and PC membranes and 600 μL was pipetted in the lower compartment of the 24-wells Transwell system which was subsequently placed in the incubator at 37 °C, 5% CO_2. The cell morphology cultured on PDMS membranes was observed daily using phase-contrast microscopy (EVOS, PA, USA). Cell viability was assessed on day 5 after seeding using a live/dead viability assay (LIVE/DEAD Viability/Cytotoxicity Kit for mammalian cells, Thermo Fisher Scientific, MA, USA) according to the manufacturer's protocol diluted together with NucBlue (two drops per milliliter, Thermo Fisher Scientific, MA, USA). The obtained fluorescence microscopy images were first processed by equalizing the window/levels as well as the brightness/contrast. After standardization of the images, the results were analyzed using the "find maxima" method on separate RFP (dead cells) and DAPI (all cells) channels in ImageJ to count the segmented cells per channel in each image.

For co-cultures, astrocytes and hCMEC/D3 cells were seeded on adjacent sides of the Transwell membrane. Again, the membranes were coated with collagen solution for 1 h at 37 °C and subsequently washed with PBS. Next, 50 μL of cell suspension (1×10^5 cells mL^{-1}) of human astrocytes in astrocyte medium (AM) with supplements (2% v/v fetal bovine serum (FBS), 1% astrocyte growth supplement (AGS, 100×), and 1% penicillin/streptomycin solution (P/S, 10 000 units mL^{-1} of penicillin and 10 000 μg mL^{-1} of streptomycin, ScienCell Research Laboratories, CA, USA) was pipetted onto the bottom side of the inverted Transwell. Astrocytes were incubated for 3 h at 37 °C, 5% CO_2 to allow them to attach to the membrane. Next, the inserts were flipped over and inserted in a Transwell plate with 600 μL of AM. The cells were incubated for another 24 h at 37 °C, 5% CO_2. A volume of 100 μL hCMEC/D3 cell suspension was added on top of the collagen-coated membranes to seed a final concentration of 15×10^4 cells mL^{-1} in endothelial cell growth medium (EGM). The medium was refreshed daily.

Immunofluorescence: Tight junctions and cell morphology were analyzed using immunofluorescence imaging. Prior to immunostaining, astrocytes and hCMEC/D3 were fixed with 4% paraformaldehyde for 20 min at room temperature (RT). After fixation, membranes were washed 3× with 1× PBS. Cells were permeated using Triton-X (0.1% in 5% bovine serum albumin (BSA) solution) for 30 min at RT. Fixed samples were incubated overnight at 4 °C with primary antibodies (ABs) in 0.5% BSA. The monoculture was probed for VE-Cadherin adherens junction (mouse monoclonal, 1:200, sc-9989, Santa Cruz Biotechnology, TX, US) and either tight-junction marker zonula occludens-1 (ZO-1, rabbit polyclonal, 1:100 dilution, 61–7300, Thermo Fisher Scientific, MA, USA) or Claudin-5 (rabbit polyclonal, 1:100, ab15106, Abcam MA, USA). The medium in the bottom compartment was replaced by 0.5% BSA in PBS. After primary AB incubation, samples were washed 3× with 1% BSA in PBS. Washed samples were incubated for 1 h at RT with Alexa Fluor 647 donkey anti-rabbit (1:500 dilution, A31573, Thermo Fisher Scientific, MA, USA) diluted together with Alexa Fluor 488 goat anti-mouse (1:200 dilution, A32723, Thermo Fisher Scientific, MA, USA) and NucBlue (two drops per milliliter, R37605, Thermo Fisher Scientific, MA, USA) in PBS. After incubation, samples were washed 3× with 1× PBS.

For co-culture staining, the same procedure was performed. After fixing the samples, primary anti-ZO-1 was pipetted in the upper compartment with endothelial cells and anti-glial fibrillary acidic protein (GFAP, 1:100 dilution, MA5-12023, mouse monoclonal, Thermo Fisher Scientific, MA, USA), was pipetted in the astrocytic compartment. The samples were incubated overnight at 4 °C and after washing, the cells were incubated with the secondary ABs (Alexa Fluor 488 anti-mouse and Alexa 647 anti-rabbit, for GFAP and ZO-1, respectively, 1:500 dilution, Thermo fisher scientific, MA, USA).

Cells were imaged using fluorescence (EVOS, PA, USA) and confocal microscopy (Nikon A1).

Scanning Electron Microscopy of Cell Samples: Cell distribution on the membranes was visualized through SEM analysis. Samples were fixed by incubation in 100% ice-cold methanol for 15 min followed by washing 2× using 1× PBS. After fixation, the samples were dehydrated using an ethanol gradient (60%, 70%, 80%, 90%, 96%, and 100% [2×] v/v ethanol in milliQ). Samples were dehydrated further using critical point drying (Blazers CPD 030) by liquid carbon dioxide exchange. Prior to the SEM analysis, the samples were gold-coated using a Cressington sputter coater. SEM images were captured using a JEOL JSM-IT 100 SEM at a 5 kV acceleration voltage.

Permeability Measurement: The integrity of the endothelial cell layer was assessed by studying the transport of fluorescently labeled dextran from the top compartment of the Transwell to the well plate. Cells were seeded as mono- and co-culture in Transwell inserts with PDMS and PC membranes as described before. Cells were cultured for 5 days to obtain a visual monolayer. Before the experiment, 600 μL of fresh medium was added to the bottom compartment of the wells plate. The medium was removed from the cell coated Transwell inserts and 100 μL of fluorescently labeled dextran (FITC-Dextran 20 kDa, Sigma Aldrich, Germany) at a concentration of 50 μg mL^{-1} was added on top of the endothelial cell layer. After 5, 15, 30, 45, and 60 min, 50 μL of the medium was sampled from the bottom compartment and transferred to a black bottom 96-well plate (Corning Inc., NY, USA). Fresh 50 μL of the medium was pipetted back to the wells to prevent pressure development over the membranes. A calibration curve was used to normalize the intensity values to the actual concentration (g mL^{-1}). Fluorescent intensity was measured using a Victor3 plate reader (PerkinElmer, Ma, USA) upon excitation at a wavelength of 485 nm and detection of emission at a wavelength of 528 nm. Results were normalized to the Transwells without cells. The empty Transwells were prepared and kept in

the same conditions as the Transwells with cells (37 °C, 5% CO_2, 5 days, refreshing the medium every day). The permeability was determined using the equations described previously with small modifications:[80]

$$P = \frac{dC}{dt}\frac{1}{C_{max}}\frac{V_a}{S_m} \quad (1)$$

$$\frac{1}{P_e} = \frac{1}{P_{tot}} - \frac{1}{P_m} \quad (2)$$

Where P is the permeability in cm s^{-1}, dC/dt is the change in the concentration (µg mL s^{-1}), C_{max} is the maximum FITC Dextran concentration added at the beginning of the experiment, V_a is the volume of the apical compartment (0.1 mL), and S_m the area of the culture membrane (0.33 cm^2).[81] To calculate the endothelial permeability P_e, the permeability of the empty Transwell P_m was subtracted from the permeability of the Transwells with cells P_{tot}.

Western Blot: The quantification of expressed proteins in hCMEC/D3 and astrocytes cultures was done by immunoblot analysis. HCMEC/D3 cells were grown in a monoculture, either with conditioned medium (CM) from an astrocyte culture or in co-culture with astrocytes for 5 days as described above. Cells were washed with ice-cold PBS and harvested from Transwells with PC and PDMS membranes by excision. Excised membranes were placed into a lysis buffer containing a protease inhibitor cocktail. Samples were then agitated at 800 rpm for 30 min at 4 °C and subsequently centrifuged for 20 min at 12 000 rpm. The total protein concentration of the resulting supernatant was quantified using a DC protein assay (Bio-Rad, CA, USA).

Equal amounts of protein were loaded onto an 8% or 10% SDS polyacrylamide gel and resolved by electrophoresis. Proteins were transferred onto polyvinylidene fluoride (PVDF) membranes (Bio-Rad, CA, USA) and blocked with either 5% non-fat dry milk (Campina, Netherlands) or 5% BSA (Sigma-Aldrich Chemie GmbH, Germany) in tris-buffered saline containing 0.05% tween-20 (TBST) for 1 h and subsequently incubated overnight at 4 °C with primary ABs dissolved in blocking buffer. The immunoblots were probed for ZO-1 (rabbit polyclonal, 1:500, Thermo Fisher Scientific, MA, USA), VE-Cadherin (mouse monoclonal, 1:1000, Santa Cruz Biotechnology, TX, US), Claudin-5 (rabbit polyclonal, 1:1000, Abcam MA, USA), and GAPDH (mouse monoclonal, 1:20 000, Merck, Germany). Blots were incubated with horseradish peroxidase-conjugated secondary ABs (1:10 000, Promega, WI, USA) for 40 min at RT.

After washing, bands were detected using a SuperSignal West Femto Chemiluminescent substrate kit (Thermo Fisher Scientific, MA, USA) and visualized using a FluorChem M imaging system (ProteinSimple, CA, USA). Band intensities were analyzed using ImageJ.

Statistical Analysis: Significance was determined by one-way ANOVA test with a post-hoc Tukey test applied when comparing more than two groups using SPSS (IBM SPSS Statistics, Version 26 for Windows), $n = 3$ per condition at each time-point in three independent experiments, a p-value of <0.05 was considered significant. For Western blot analysis, different groups were compared: PDMS mono vs CM vs co; PC mono vs CM vs co; PDMS mono vs PC mono; PDMS CM vs PC CM and PDMS co vs PC co. The graphs were plotted using Prism Graph Pad.

Supporting Information

Supporting Information is available from the Wiley Online Library or from the author.

Acknowledgements

M.Z. and M.P.T. contributed equally to this work. This work was supported by the Netherlands Organ-on-Chip Initiative, an NWO Gravitation project (024.003.001) funded by the Ministry of Education, Culture and Science of the government of the Netherlands (to Prof. Albert van den Berg). The authors also acknowledge the European Research Council advanced grant VESCEL (grant number 669768 Prof. Albert van den Berg).

Conflict of Interest

The authors declare no conflict of interest.

Data Availability Statement

The data that support the findings of this study are available from the corresponding author upon reasonable request.

Keywords

2 µm thin polydimethylsiloxane membrane, blood-brain barrier, co-culture, commercial polycarbonate membrane, permeability assay, protein expression, transwell

Received: February 4, 2021
Revised: June 25, 2021
Published online:

[1] J. H. George, S. T. Waller, H. Ye, *Transwell-Integrated 2 µm Thick Transparent Polydimethylsiloxane Membranes with Controlled Pore Sizes and Distribution to Model the Blood-Brain Barrier*, Elsevier, New York **2017**, pp. 272–292.
[2] A. D. van der Meer, A. van den Berg, *Integr. Biol.* **2012**, *4*, 461.
[3] S. Hosic, A. J. Bindas, M. L. Puzan, W. Lake, J. R. Soucy, F. Zhou, R. A. Koppes, D. T. Breault, S. K. Murthy, A. N. Koppes, *ACS Biomater. Sci. Eng.* **2020**, *7*, 2949.
[4] A. K. H. Achyuta, A. J. Conway, R. B. Crouse, E. C. Bannister, R. N. Lee, C. P. Katnik, A. A. Behensky, J. Cuevas, S. S. Sundaram, *Lab Chip* **2013**, *13*, 542.
[5] J. H. George, D. Nagel, S. Waller, E. Hill, H. R. Parri, M. D. Coleman, Z. Cui, H. Ye, *Sci. Rep.* **2018**, *8*, 15552.
[6] J. A. Brown, V. Pensabene, D. A. Markov, V. Allwardt, M. Diana Neely, M. Shi, C. M. Britt, O. S. Hoilett, Q. Yang, B. M. Brewer, P. C. Samson, L. J. McCawley, J. M. May, D. J. Webb, D. Li, A. B. Bowman, R. S. Reiserer, J. P. Wikswo, *Biomicrofluidics* **2015**, *9*, 054124.
[7] T. E. Park, N. Mustafaoglu, A. Herland, R. Hasselkus, R. Mannix, E. A. FitzGerald, R. Prantil-Baun, A. Watters, O. Henry, M. Benz, H. Sanchez, H. J. McCrea, L. C. Goumnerova, H. W. Song, S. P. Palecek, E. Shusta, D. E. Ingber, *Nat. Commun.* **2019**, *10*, 2621.
[8] F. R. Walter, S. Valkai, A. Kincses, A. Petneházi, T. Czeller, S. Veszelka, P. Ormos, M. A. Deli, A. Dér, *Sensors Actuators, B Chem.* **2016**, *222*, 1209.
[9] O. Y. F. Henry, R. Villenave, M. J. Cronce, W. D. Leineweber, M. A. Benz, D. E. Ingber, *Lab Chip* **2017**, *17*, 2264.
[10] N. L. Stone, T. J. England, S. E. O'Sullivan, *Front. Cell. Neurosci.* **2019**, *13*, 230.
[11] E. Vandenhaute, A. Drolez, E. Sevin, F. Gosselet, C. Mysiorek, M.-P. Dehouck, *Lab. Investig.* **2016**, *96*, 588.
[12] C. F. Kuo, S. Majd, *Proc. Annu. Int. Conf. IEEE Eng. Med. Biol. Soc. EMBS* **2020**, 3331.
[13] H. C. Helms, N. J. Abbott, M. Burek, R. Cecchelli, P.-O. Couraud, M. A. Deli, C. Förster, H. J. Galla, I. A. Romero, E. V Shusta, M. J. Stebbins, E. Vandenhaute, B. Weksler, B. Brodin, J. Cereb, *Blood Flow Metab.* **2016**, *36*, 862.
[14] J. H. Tao-Cheng, Z. Nagy, M. W. Brightman, *J. Neurosci.* **1987**, *7*, 3293.
[15] P. Demeuse, A. Kerkhofs, C. Struys-Ponsar, B. Knoops, C. Remacle, P. Van Den, Bosch DeAguilar , *J. Neurosci. Methods* **2002**, *121*, 21.

[16] C. Kulczar, K. E. Lubin, S. Lefebvre, D. W. Miller, G. T. Knipp, *J. Pharm. Pharmacol.* **2017**, *69*, 1684.
[17] M. S. Thomsen, S. Birkelund, A. Burkhart, A. Stensballe, T. Moos, *J. Neurochem.* **2017**, *140*, 741.
[18] M. D. Sweeney, S. Ayyadurai, B. V. Zlokovic, *Nat. Neurosci.* **2016**, *19*, 771.
[19] J. S. Harunaga, A. D. Doyle, K. M. Yamada, *Dev. Biol.* **2014**, *394*, 197.
[20] D. Kim, S. Eom, S. M. Park, H. Hong, D. S. Kim, *Sci. Rep.* **2019**, *9*, 14915.
[21] J. Yoo, T. H. Kim, S. Park, K. Char, S. H. Kim, J. J. Chung, Y. Jung, *Adv. Funct. Mater.* **2021**, *31*, 2008172.
[22] C. Drieschner, M. Minghetti, S. Wu, P. Renaud, K. Schirmer, *ACS Appl. Mater. Interfaces* **2017**, *9*, 9496.
[23] A. R. Mazzocchi, A. J. Man, J. P. S. DesOrmeaux, T. R. Gaborski, *Cell. Mol. Bioeng.* **2014**, *7*, 369.
[24] S. H. Ma, L. A. Lepak, R. J. Hussain, W. Shain, M. L. Shuler, *Lab Chip* **2005**, *5*, 74.
[25] C. Drieschner, S. Könemann, P. Renaud, K. Schirmer, *Lab Chip* **2019**, *19*, 3268.
[26] S. Gholizadeh, Z. Allahyari, R. N. Carter, L. F. Delgadillo, M. Blaquiere, F. Nouguier-Morin, N. Marchi, T. R. Gaborski, *Adv. Mater. Technol.* **2020**, *5*, 2000474.
[27] R. N. Carter, S. M. Casillo, A. R. Mazzocchi, J. P. S. Desormeaux, J. A. Roussie, T. R. Gaborski, *Biofabrication* **2017**, *9*, 015019.
[28] B. J. Nehilla, N. Nataraj, T. R. Gaborski, J. L. McGrath, *Acta Biomater.* **2014**, *10*, 4670.
[29] A. Mossu, M. Rosito, T. Khire, H. Li Chung, H. Nishihara, I. Gruber, E. Luke, L. Dehouck, F. Sallusto, F. Gosselet, J. L. McGrath, B. Engelhardt, J. Cereb, *Blood Flow Metab.* **2019**, *39*, 395.
[30] S. R. Gillmer, D. Z. Fang, S. E. Wayson, J. D. Winans, N. Abdolrahim, J. P. S. DesOrmeaux, J. Getpreecharsawas, J. D. Ellis, P. M. Fauchet, J. L. McGrath, *Thin Solid Films* **2017**, *631*, 152.
[31] Y. Yang, K. Wang, X. Gu, K. W. Leong, *Engineering* **2017**, *3*, 36.
[32] E. E. Bastounis, Y. T. Yeh, J. A. Theriot, *Sci. Rep.* **2019**, *9*, 18209.
[33] A. Skardal, D. Mack, A. Atala, S. Sokern, *J. Mech. Behav. Biomed. Mater.* **2013**, *17*, 307.
[34] P. A. Janmey, D. A. Fletcher, C. A. Reinhart-King, *Physiol. Rev.* **2020**, *100*, 695.
[35] D. E. Discher, P. Janmey, Y. L. Wang, *Science (80-.)*. **2005**, *310*, 1139.
[36] D. T. Butcher, T. Alliston, V. M. Weaver, *Nat. Rev. Cancer* **2009**, *9*, 108.
[37] Z. Gan, C. Wang, Z. Chen, *Surfaces* **2018**, *1*, 59.
[38] A. K. Katiyar, A. A. Davidson, H. Jang, Y. Hwangbo, B. Han, S. Lee, Y. Hagiwara, T. Shimada, H. Hirakata, T. Kitamura, J. H. Ahn, *Nanoscale* **2019**, *11*, 15184.
[39] H. H. Chung, M. Mireles, B. J. Kwarta, T. R. Gaborski, *Lab Chip* **2018**, *18*, 1671.
[40] W. F. Quirós-Solano, N. Gaio, O. M. J. A. Stassen, Y. B. Arik, C. Silvestri, N. C. A. Van Engeland, A. Van der Meer, R. Passier, C. M. Sahlgren, C. V. C. Bouten, A. van den Berg, R. Dekker, P. M. Sarro, *Sci. Rep.* **2018**, *8*, 13524.
[41] H. Le-The, M. Tibbe, J. Loessberg-Zahl, M. P. do Carmo, M. van der Helm, J. Bomer, A. van den Berg, A. Leferink, L. Segerink, J. Eijkel, *Nanoscale* **2018**, *10*, 7711.
[42] M. Zakharova, M. P. do Carmo, M. van der Helm, H. Le-The, M. N. S. de graaf, V. Orlova, A. van den Berg, A. D. van der Meer, K. Broersen, L. I. Segerink, *Lab Chip* **2020**, *20*, 3132.
[43] N. J. Abbott, L. Rönnbäck, E. Hansson, *Nat. Rev. Neurosci.* **2006**, *7*, 41.
[44] E. A. Winkler, R. D. Bell, B. V. Zlokovic, *Nat. Neurosci.* **2011**, *14*, 1398.
[45] S. W. Lee, W. J. Kim, Y. K. Choi, H. S. Song, M. J. Son, I. H. Gelman, Y. J. Kim, K. W. Kim, *Nat. Med.* **2003**, *9*, 900.
[46] H. H. Tsai, H. Li, L. C. Fuentealba, A. V. Molofsky, R. Taveira-Marques, H. Zhuang, A. Tenney, A. T. Murnen, S. P. J. Fancy, F. Merkle, N. Kessaris, A. Alvarez-Buylla, W. D. Richardson, D. H. Rowitch, *Science (80-.)*. **2012**, *337*, 358.
[47] R. Booth, H. Kim, *Lab Chip* **2012**, *12*, 1784.
[48] S. I. Ahn, Y. J. Sei, H. J. Park, J. Kim, Y. Ryu, J. J. Choi, H. J. Sung, T. J. MacDonald, A. I. Levey, Y. Kim, *Nat. Commun.* **2020**, *11*, 175.
[49] S. M. Casillo, A. P. Peredo, S. J. Perry, H. H. Chung, T. R. Gaborski, *ACS Biomater. Sci. Eng.* **2017**, *3*, 243.
[50] P. D. Yurchenco, *Cold Spring Harb. Perspect. Biol.* **2011**, *3*, a004911.
[51] L. Xu, A. Nirwane, Y. Yao, *Stroke Vasc. Neurol.* **2019**, *4*, 78.
[52] R. D. Hurst, I. B. Fritz, *J. Cell. Physiol.* **1996**, *167*, 81.
[53] K. Sobue, N. Yamamoto, K. Yoneda, M. E. Hodgson, K. Yamashiro, N. Tsuruoka, T. Tsuda, H. Katsuya, Y. Miura, K. Asai, T. Kato, *Neurosci. Res.* **1999**, *35*, 155.
[54] N. J. Abbott, *J. Anat.* **2002**, *200*, 629.
[55] L. M. Griep, F. Wolbers, B. De Wagenaar, P. M. Ter Braak, B. B. Weksler, I. A. Romero, P. O. Couraud, I. Vermes, A. D. Van Der Meer, A. Van Den Berg, *Biomed. Microdevices* **2013**, *15*, 145.
[56] E. Urich, S. E. Lazic, J. Molnos, I. Wells, P.-O. Freskgård, *PLoS One* **2012**, *7*, e38149.
[57] E. A. L. M. Biemans, L. Jäkel, R. M. W. de Waal, H. B. Kuiperij, M. M. Verbeek, *J. Neurosci. Res.* **2017**, *95*, 1513.
[58] L. N. Handly, A. Pilko, R. Wollman, *eLife* **2015**, *4*, e09652.
[59] B. B. Weksler, E. A. Subileau, N. Perrière, P. Charneau, K. Holloway, M. Leveque, H. Tricoire-Leignel, A. Nicotra, S. Bourdoulous, P. Turowski, D. K. Male, F. Roux, J. Greenwood, I. A. Romero, P. O. Couraud, *FASEB J.* **2005**, *19*, 1872.
[60] K. Umeda, J. Ikenouchi, S. Katahira-Tayama, K. Furuse, H. Sasaki, M. Nakayama, T. Matsui, S. Tsukita, M. Furuse, S. Tsukita, *Cell* **2006**, *126*, 741.
[61] O. Beutel, R. Maraspini, K. Pombo-García, C. Martin-Lemaitre, A. Honigmann, *Cell* **2019**, *179*, 923.
[62] C. Schwayer, S. Shamipour, K. Pranjic-Ferscha, A. Schauer, M. Balda, M. Tada, K. Matter, C. P. Heisenberg, *Cell* **2019**, *179*, 937.
[63] S. Varadarajan, R. E. Stephenson, A. L. Miller, *J. Cell Sci.* **2019**, *132*, jcs22986.
[64] F. Ataollahi, S. Pramanik, A. Moradi, A. Dalilottojari, B. Pingguan-Murphy, W. A. B. W. Abas, N. A. A. Osman, *J. Biomed. Mater. Res. – Part A* **2015**, *103*, 2203.
[65] A. J. Haas, C. Zihni, A. Ruppel, C. Hartmann, K. Ebnet, M. Tada, M. S. Balda, K. Matter, *Cell Rep.* **2020**, *32*, 107924.
[66] A. Angulo-Urarte, T. van der Wal, S. Huveneers, *Biochim. Biophys. Acta – Biomembr.* **2020**, *1862*, 183316.
[67] G. Adriani, D. Ma, A. Pavesi, R. D. Kamm, E. L. K. Goh, *Lab Chip* **2017**, *17*, 448.
[68] O. C. Colgan, N. T. Collins, G. Ferguson, R. P. Murphy, Y. A. Birney, P. A. Cahill, P. M. Cummins, *Brain Res.* **2008**, *1193*, 84.
[69] B. P. Heithoff, K. K. George, A. N. Phares, I. A. Zuidhoek, C. Munoz-Ballester, S. Robel, *Glia* **2021**, *69*, 436.
[70] S. Nakagawa, M. A. Deli, H. Kawaguchi, T. Shimizudani, T. Shimono, Á. Kittel, K. Tanaka, M. Niwa, *Neurochem. Int.* **2009**, *54*, 253.
[71] E. A. L. M. Biemans, L. J. Akel, R. M. W. De Waal, H. B. Kuiperij, M. M. Verbeek, *J. Neurosci. Res.* **2017**, *95*, 1513.
[72] R. C. A. Eguiluz, K. B. Kaylan, G. H. Underhill, D. E. Leckband, *Biomaterials* **2017**, *140*, 45.
[73] M. S. Balda, K. Matter, *Biochim. Biophys. Acta – Biomembr.* **2009**, *1788*, 761.
[74] T. W. Gardner, E. Lieth, S. A. Khin, A. J. Barber, D. J. Bonsall, T. Lesher, K. Rice, W. A. BrennanJr, *Invest. Ophthalmol. Visual Sci.* **1997**, *38*, 2423.
[75] N. R. Wevers, H. E. de Vries, *Tissue Barriers* **2016**, *4*, e1090524.
[76] R. C. Brown, A. P. Morris, R. G. O'Neil, *Brain Res.* **2007**, *1130*, 17.
[77] F. Idris, S. H. Muharram, Z. Zaini, S. Diah, *bioRxiv* **2018**, 435990.
[78] Y. I. Wang, H. E. Abaci, M. L. Shuler, *Biotechnol. Bioeng.* **2017**, *114*, 184.
[79] S. Bang, S. R. Lee, J. Ko, K. Son, D. Tahk, J. Ahn, C. Im, N. L. Jeon, *Sci. Rep.* **2017**, *7*, 8083.
[80] H. Yuan, M. W. Gaber, T. McColgan, M. D. Naimark, M. F. Kiani, T. E. Merchant, *Brain Res.* **2003**, *969*, 59.
[81] M. P. Dehouck, P. Jolliet-Riant, F. Brée, J. C. Fruchart, R. Cecchelli, J. P. Tillement, *J. Neurochem.* **1992**, *58*, 1790.